Damage processes and magnetic field orientation in ferrimagnetic oxides $Y_3Fe_5O_{12}$ and $BaFe_{12}O_{19}$ irradiated by high-energy heavy ions: A Mössbauer study

M. Toulemonde and G. Fuchs*
Centre Interdisciplinaire de Recherches avec les Ions Lourds (CIRIL), Boite Postale 5133, 14040 Caen Cédex, France

N. Nguyen, F. Studer, and D. Groult
Laboratoire de Cristallographie et sciences des materiause
Institut des sciences de la Matiere et due Rayonnement (ISMRa)
Boulevard du Maréchal Juin, 14032 Caen Cédex, France

(Received 24 November 1986)

Mössbauer spectroscopy of damage induced by energetic Ar, Kr, and Xe ions in the giga-electron-volt range in two ferrimagnetic oxides, $Y_3Fe_5O_{12}$ and $BaFe_{12}O_{19}$, is presented. The enhancement of the paramagnetic phase observed after an irradiation with high-energy deposition (Xe and Kr ions) compared to low-energy deposition (Ar ions) supports a damage mechanism based on the electronic stopping power. Threshold energy-deposition values close to 17 and 25 MeV cm^2 mg^{-1} have thus been determined for $Y_3Fe_5O_{12}$ and $BaFe_{12}O_{19}$, respectively. Furthermore, drastic changes in the bulk orientation of the hyperfine magnetic field H_f have been observed in yttrium iron garnet: The H_f distribution is isotropic for Ar irradiations and anisotropic for Xe irradiations, while two types of H_f distributions are observed for Kr irradiations, depending on the values of the deposited energy compared to that of the threshold energy. Comparison with latent-track models is performed.

I. INTRODUCTION

High-energy heavy ions in insulators leave discontinuous[1,2] or continuous[3,4] trails of damaged regions in their wakes called latent tracks. The dependence of the track shape and diameter upon the energy and mass of the incident ions is linked with the energy loss of heavy ions in solids.[1,3,5,6]

The creation of such tracks have been already reported in garnet thin films irradiated with Xe and U ions having energies around 0.5 GeV.[7,8] However, more recently irradiations of ferrimagnetic oxides $Y_3Fe_5O_{12}$ and $BaFe_{12}O_{19}$ by Ar ions of 1.8 GeV (Refs. 9 and 10) have shown that drastic changes in magnetic properties cannot be interpreted on the assumption of a continuous trail of damage on account of unrealistic values of the track radii compared to previous experimental determinations.[3,4] As a consequence, a threshold energy deposition for the formation of tracks is expected in such materials, as it has been recently shown[11–13] in $Y_3Fe_5O_{12}$. In order to get more information about this phenomenon, special attention has been focused on a Mössbauer study of $Y_3Fe_5O_{12}$ and $BaFe_{12}O_{19}$ magnetic oxides irradiated by Ar, Kr, and Xe GeV-energy ion beams. Such a study offers, with regard to magnetization measurements and high-resolution electron microscopy previously reported,[14] new possibilities to elucidate the effects induced by the increase of the electronic stopping power.[12]

II. EXPERIMENT

A. Irradiation procedure

The experiments were performed at GANIL with 1.8-GeV Ar, 2.7- and 3.5- GeV Kr, and 3-GeV Xe using the IRABAT facility.[15] The irradiated surface of the target was defined with a good accuracy by means of a sweeping magnet[16] and adjustable slits placed along the ion-beam path. A surface of 25×25 mm^2 can thus be homogeneously irradiated.

The fluences were evaluated during the irradiation from the current measured on a thin tantalum foil located between the target and the slits. Before irradiation a calibration of the current deposited by the ions passing through the tantalum foil was realized by means of a Faraday cup. The average fluxes were about 5×10^8, 10^9, and 3×10^{10} ions cm^{-2} s^{-1} for Xe, Kr, and Ar ions, respectively.

The sample holders were fixed on the IRABAT tail as previously described[9–11] and contained either three or seven stacks of thin disks of polycrystalline sinter and single-crystal $\langle111\rangle$-oriented $Y_3Fe_5O_{12}$ and $\langle001\rangle$-oriented $BaFe_{12}O_{19}$. However, it must be pointed out that, for these last experiments, the sample holders were modified in order to avoid any correction for the irradiated surface: In the first experiments, the irradiated surface was limited by collimators to 50% or 75% of the total sample area. In the new ones, a thin foil of Al (12-μm thick) glued on the surface of the sample holder maintained the stacks in front of the ion beams.

The irradiation was always performed perpendicularly to the surface of the samples. In order to adjust the mean energy deposited inside each disk of a stack, calibrated disks of Al were intercalated between every two disks. As noted elsewhere,[9,10] the thickness of the stack has been adjusted with respect to the projected range of the ions, namely 670, 350, and 160 μm for Ar, Kr, and Xe ions, respectively. These ranges have been verified by radioactivity measurements.[17] The macroscopic physical properties measured by Mössbauer spectroscopy and magnetization[9,10] have thus been corrected for the effective irradiated volume. The experiments were carried out in a cryostat cooled by liquid nitrogen for Ar, Kr, and Xe irradia-

tions and at room temperature for Kr and Xe only. The temperature was measured during the irradiation by a copper-Constantan thermocouple located inside the sample holder. For Ar experiments, the intensity of the beam was limited to 10^{11} ions cm^{-2} s^{-1} in order to maintain the sample-holder temperature below 160 K during the irradiation.

B. Mössbauer experiment

The Mössbauer spectra were recorded using the standard absorption method at room temperature, except as otherwise stated. A ^{57}Co-in-Rh source was placed on a constant-acceleration spectrometer. The emitted γ rays were collimated by a hole drilled in a 5-mm-thick lead disk and placed at a distance of 100 mm from the source. The hole diameter took into account the diameter of the sample to be analyzed. The thickness of the sample ranged between 50 and 150 μm in order to reduce the γ-ray absorption and to obtain the best signal-to-background ratio.

The ^{57}Fe Mössbauer spectrum gives quantitative information on the hyperfine magnetic field at the iron nuclei. From the intensity ratio of the peaks, the direction of the hyperfine magnetic field and thus of the magnetization can be deduced. The intensities of the outer (A), middle (B), and inner (C) pairs of the peaks in a magnetic sextuplet can be expressed as $A:B:C$ equal to $3(1+\cos^2\theta):4\sin^2\theta:1+\cos^2\theta$, where θ is the angle between the incident γ rays and the hyperfine magnetic field. In this work, the γ rays were perpendicular to the surface of the samples and consequently parallel to the heavy-ion beam, except when otherwise stated. In the case of polycrystalline sintered samples, the relative intensities will be in the ratios $A:B:C$ equal to 3:2:1 if we consider an isotropic distribution of the hyperfine magnetic field. For the $\langle 111\rangle$-oriented $Y_3Fe_5O_{12}$ and $\langle 001\rangle$-oriented $BaFe_{12}O_{19}$ single crystals, the relative intensities will be 3:0:1 since the axis is the easy-magnetization one.[18–20] These last cases correspond typically to an anisotropic distribution of the hyperfine magnetic field. In order to evaluate the fraction of the disk which has been damaged, the observed spectra were least-squares-fitted using the program MOSFIT written by F. Varet and J. Teillet of Université du Maine, France. As expected, the Mössbauer spectra of the nonirradiated oxides[21] are in agreement with the previous theoretical predictions[18–20] and experimental results, taking into account the crystallographic sites of iron in $Y_3Fe_5O_{12}$ and $BaFe_{12}O_{19}$.

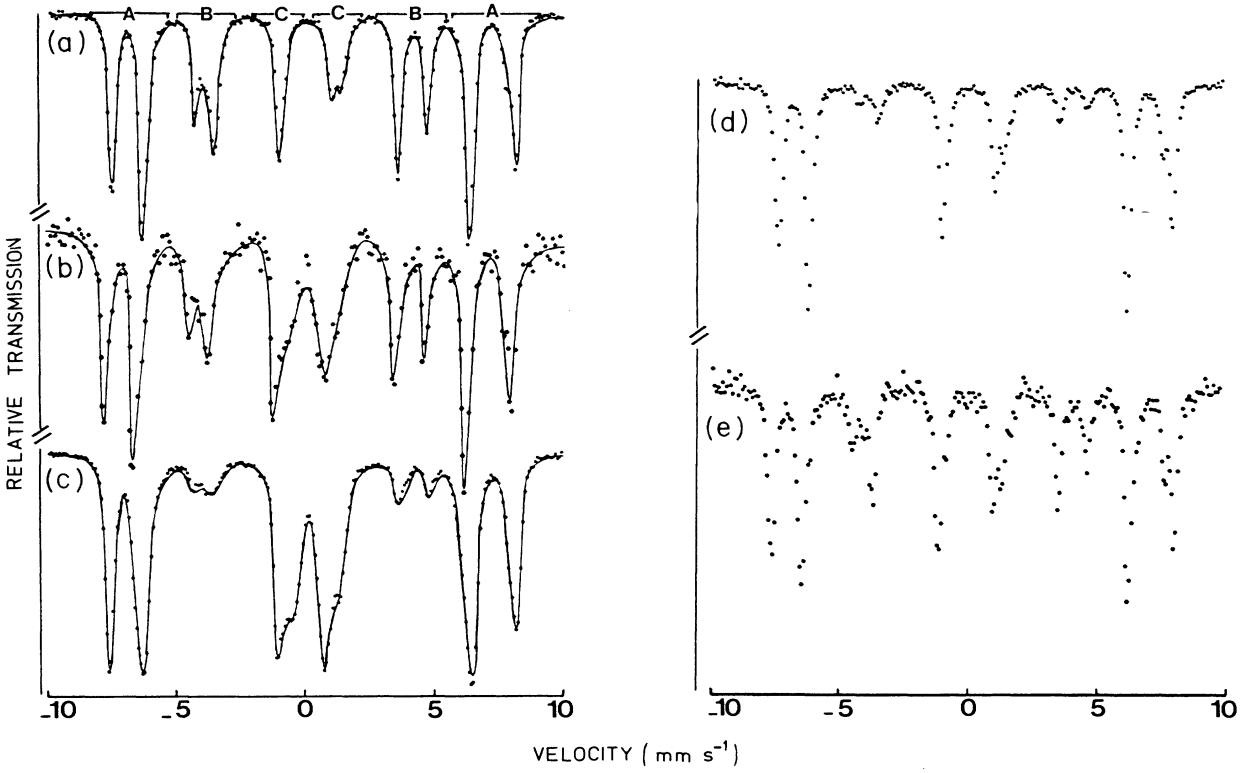

FIG. 1. Ar and Xe irradiations of $Y_3Fe_5O_{12}$ samples. All the spectra were recorded with the samples at 300 K. (a) Nonirradiated polycrystalline sinter. (b) Ar irradiation of polycrystalline sinter; $\phi t = 6\times10^{14}$ cm^{-2}; $0.85 > E > 0.24$ GeV; half of the surface was irradiated (see Ref. 9); $F_d = 17\%$. (c) Xe irradiation of polycrystal; $\phi t = 3.5\times10^{11}$ cm^{-2}; $3.0 > E > 0.7$ GeV; $F_d = 32\%$. (d) Nonirradiated $\langle 111\rangle$ single crystal; it should be noted that the samples were cut perpendicularly to a $\langle 111\rangle$ direction of the garnet oriented by x-ray diffraction. Despite that, weaker intensity of the lines B still remains. (e) Ar irradiation of $\langle 111\rangle$ single crystal; $\phi t = 2.5\times10^{14}$ cm^{-2}; $1.2 > E > 0.24$ GeV; three-quarters of the surface of the sample was irradiated (see Ref. 9); $F_d < 5\%$.

III. RESULTS IN $Y_3Fe_5O_{12}$

A. Mössbauer study

The Mössbauer spectra of irradiated polycrystalline sinters and ⟨111⟩ single crystals are reported in Figs. 1 and 2. As shown elsewhere,[8] the radiation damage results in a paramagnetic fraction which appears in the form of a doublet in the middle part of the spectra [Fig. 1(b) compared to Fig. 1(a)]. Whatever the irradiation, the remaining magnetic part of the samples shows no change in H_f nor in the distribution of Fe^{3+} ions in both octahedral and tetrahedral sites. Besides this effect, a drastic change in the intensity ratio of the lines A and B can also be observed. It involves a change in the orientation of the hyperfine magnetic field (H_f) strongly depending on the atomic number of the incident ions.

1. Argon irradiations

This effect is clearly visible on Fig. 1(e), which shows, compared to Fig. 1(d), the enhancement of the lines B and hence the increase of the ratio $B:A$ for a ⟨111⟩ irradiated single crystal. It is confirmed by the recording of the spectra at angles of 55° and 45° relative to the surface of the sample. In all cases, the fit of the spectra can only be obtained if one considers the sum of three contributions corresponding to (i) the initial spectrum [Fig. 1(d)], (ii) a paramagnetic fraction, and (iii) an isotropic distribution of the hyperfine field. Therefore, it may be concluded that argon-ion bombardment results in a paramagnetic fraction and an isotropic distribution of the magnetic field.

The conclusion is corroborated by the Mössbauer study of polycrystalline sinters, which show effectively no change of the ratio $B:A$, the value equal to 0.6 [Fig. 1(b)], being consistent with an isotropic distribution of H_f for the remaining magnetic part of the sample.

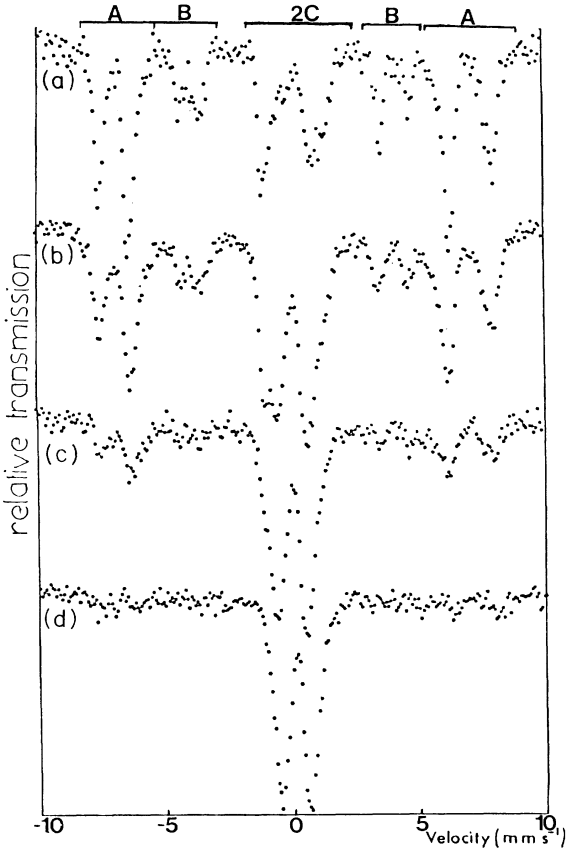

FIG. 2. Kr irradiation of polycrystalline sinters $Y_3Fe_5O_{12}$ (see Table I). (a) sample 10, (b) sample 11, (c) sample 12, and (d) sample 13.

2. Xenon irradiations

Contrary to the case for argon ions, it can be seen in Fig. 1(c) that the irradiation of polycrystalline sinters by xenon ions has induced, in addition to the appearance of the paramagnetic fraction, an anisotropic distribution of the hyperfine magnetic field indicated by a decrease of the intensity of the lines B compared to the intensity of the lines A. The direction of the hyperfine magnetic field is assumed to be parallel to the ion path. Such assumption is confirmed by recording Mössbauer spectra at different angles (35° and 55°) relative to the γ ray direction. Moreover, the paramagnetic fraction appears at a fluence 3 orders of magnitude less than that for Ar ions.

3. Krypton irradiations

Two incident energies have been considered, 2.7 and 3.5 GeV. The results are summarized in Table I for both energies. Figure 2 shows the Mössbauer spectra of polycrystalline sinters corresponding to the last four samples of the stack irradiated with 3.5-GeV Kr ions (samples 10–13, Table I). A transition from a ferrimagnetic state up to a nearly complete paramagnetic state is clearly established, depending on the location of the sample in the stack with respect to the deposited energy. Moreover, a decrease of the relative intensity of the lines B compared to that of the lines A can also be observed for the irradiated polycrystalline sinters, as mentioned above for xenon irradiations. One experiment, performed at 2.7 GeV incident energy on a ⟨111⟩-oriented single crystal, shows also a decrease of the weak intensities of the lines B, compared to the line A. Such induced anisotropy in the distribution of the hyperfine magnetic field is therefore a result of the irradiation. On the other hand, an increase of the intensities of the lines B relative to that of the lines A is observed on the Mössbauer spectra of a single crystal.[22] The first sample of the stack irradiated by 3.5 GeV Kr ions (Table I, sample 9) implies a change in the damage creation at higher energy.

B. Paramagnetic fraction

As the transition temperature of the amorphous $Y_3Fe_5O_{12}$ from magnetic order up to the paramagnetic order is 70 K,[21] the fraction of disordered matter, F_d called the paramagnetic fraction, can be directly determined from the lines areas: if A, B, and C are the areas of the

TABLE I. Results of krypton irradiations of $Y_3Fe_5O_{12}$ samples.

Samples	Fluences ϕt (10^{13} ions/cm^2)	Temperature of irradiation T (K)	Energy in E_i (MeV)	Energy out E_o (MeV)	Paramagnetic phase F_d (%)	Oriented phase F_o (%)
1[a]	2	130	2713	1302	27±3	38±4
2	2	130	1302	84	100±10	
3[a]	4	120	2713	1663	51±5	49±5
4	4	120	1570	588	100±10	
5[b]	1.6	110	2301	1352	13±2	42±4
6[b]	1.6	110	1988	1016	32±3	43±4
7[b]	1.6	110	1579	504	84±9	16±2
8[b]	1.6	110	1252	20	100±10	
9[a]	2	350	3536	2856	3.4±1.0	33±3[c]
10	2	350	2788	2268	13±2	38±4
11	2	350	2209	1612	37±4	33±4
12	2	350	1545	840	65±6	35±4
13	2	350	722	0	100±10	

[a]Same stacks.
[b]On the same sample holder, but for different stacks, the incident energy was determined by the calibrated thickness of aluminum degraders.
[c]This value corresponds to an isotropic distribution of the hyperfine magnetic field contrary to all the other values, which correspond to a magnetic hyperfine field parallel to the heavy-ion path.
[d]The errors are characteristics of all the data obtained from the Mössbauer study. It should be mentioned here that the relative error on the fluence t is only dependent of the sweeping homogeneity of the beam for the same stack of samples.

outer, inner, and central lines, respectively, the paramagnetic fraction can indeed be expressed as $F_d = (C - A/3)/(A + B + C)$. The results are in agreement with that deduced from the magnetization measurements[9,10] within an experimental error of 10%, which does not allow us to confirm or to contradict the systematic difference observed by Hansen *et al.*[8] between the two measurements. Accordingly, the averaged values of F_d, obtained from the decrease of the saturation magnetization and from the Mössbauer study, have been considered and plotted as in Ref. 12 against the number of displacements per atom, N_d/N_t, in Fig. 3(a).

For the temperature range investigated, the effect of the temperature has been found to be negligible for xenon irradiations and also for Kr irradiations (Table I), as can be seen if the damage rate obtained from F_d and F_o (Table I) and referred to the same fluences is plotted against the electronic stopping power (Fig. 4). F_o defined as $F_o = (4A/3 - 2B)/(A + B + C)$ is directly related to the volumic fraction of the irradiated sample evidencing a hyperfine field parallel to the γ rays.

IV. RESULTS IN $BaFe_{12}O_{19}$

A. Mössbauer study

Figure 5 shows the Mössbauer spectra obtained at 300 and 450 K in ⟨001⟩-oriented single crystals irradiated

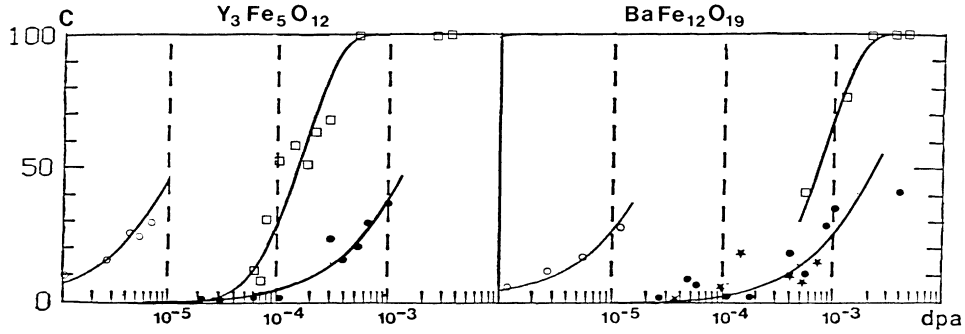

FIG. 3. F_d, disordered material fraction or paramagnetic fraction, vs N_d/N_t induced by Ar,Kr,Xe irradiations for (a) $Y_3Fe_5O_{12}$ and (b) $BaFe_{12}O_{19}$. Ar (●), Kr (□), Xe (○) for $Y_3Fe_5O_{12}$. Az (●), Kr <1.1 GeV (□), Kr >1.1 GeV (*), Xe (○) for $BaFe_{12}O_{19}$. The lines are only drawn to guide the eye. The number N_d/N_t has been calculated (Ref. 12) following the model proposed by Norgett *et al.* (Ref. 23) and is based on the atomic displacement after an elastic collision. The relative error on N_d/N_t has been estimated equal to ±0.15 owing to the measurement of the fluence.

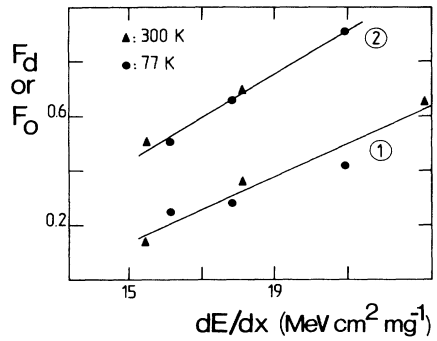

FIG. 4. Percentage of the magnetic properties change versus the electronic stopping power for two irradiation temperatures. Curve 1 corresponds only to the paramagnetic phase of krypton irradiation in $Y_3Fe_5O_{12}$. Curve 2 corresponds to the paramagnetic phase plus the oriented phase. These values are extracted from Table I and normalized for the same fluences. The lines are to guide the eye.

with xenon and krypton ions. As already noted, the effect of the ion bombardments consists of a vanishing of the magnetic sextuplet due to Fe^{3+} ions in $4f$ and $12k$ crystallographic sites in nonirradiated $BaFe_{12}O_{19}$ samples [Fig. (5a)] and the appearance of a paramagnetic doublet in the middle of the spectra [Fig. 5(b)]. As expected, the area of the doublet increases with the fluence [Figs. 5(c) and 5(d)]. Furthermore, as shown in Fig. 5(e), a paramagnetic phase is obtained when the Mössbauer spectrum is recorded at 450 K. Therefore, it has been assumed that the Mössbauer spectrum recorded at room temperature [Fig. 5(d)] corresponds to a phase transition up to a magnetic order which seems, however, to be observed when the fraction of the disordered matter is approximately higher than 50%. As a consequence, the spectrum pictured in Fig. 5(c) has been least-squares-fitted by means of a linear combination of Figs. 5(a) and 5(d) at room temperature.

In a similar way, the Mössbauer spectra reported in Fig. 6 for polycrystalline sinters of $BaFe_{12}O_{19}$ irradiated with Ar, Kr, and Xe ions have been carefully analyzed, accounting for such a transition up to a magnetic order, as can be seen in Fig. 6(c).

B. Disordered fraction F_d

The values of F_d calculated from the Mössbauer spectra are in good agreement with those obtained from the magnetization measurements for argon[9] and xenon ions. In the case of Xe ions the effect of the irradiation temperature has been found, as in $Y_3Fe_5O_{12}$, to be negligible. The averaged values of F_d have thus been reported in Fig. 3(b).

For krypton irradiations, significant differences between

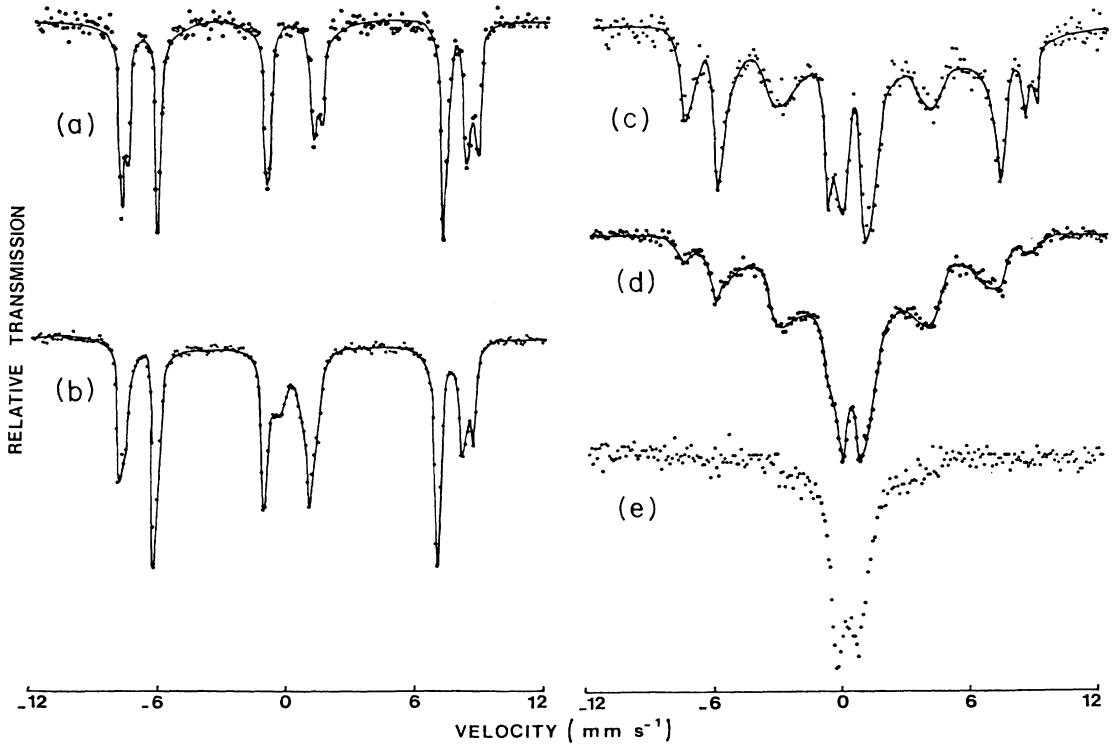

FIG. 5. Mössbauer spectra of ⟨001⟩-oriented $BaFe_{12}O_{19}$ single crystal recorded with the samples at 300 K, except for (e). E is the energy of the incident ions. F_d is the fraction of disordered material. (a) Nonirradiated. (b) Xe irradiation; $\phi t = 3.5 \times 10^{11}$ cm^{-2}; $3.0 > E > 1.2$ GeV; $F_d = 24\%$. (c) Kr irradiation; $\phi t = 1.6 \times 10^{13}$ cm^{-2}; $1.5 > E > 0.1$ GeV; $F_d = 75\%$. (d) Kr irradiation; $\phi t = 10^{14} \times$ cm^{-2}; $1.5 > E > 0$ GeV; the sample was at 300 K during the Mössbauer accumulation. $F_d = 100\%$. (e) Same sample as (d), but the Mössbauer spectrum was recorded with the sample at 450 K. $F_d = 100\%$.

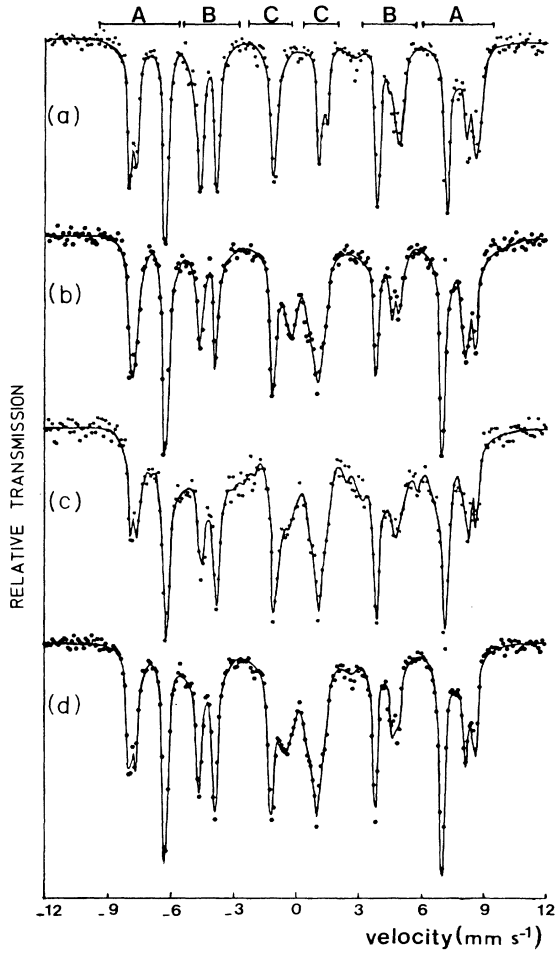

FIG. 6. Mössbauer spectra of polycrystalline sinters of $BaFe_{12}O_{19}$ all registered with the sample at 300 K. (a) Nonirradiated sample. (b) Ar irradiation; $\phi t = 6 \times 10^{14}$ cm^{-2}; $0.75 > E > 0$ GeV; only half of the surface of the sample was irradiated (see Ref. 9); $F_d = 20\%$. (c) Kr irradiation; $\phi t = 10^{13} \times$ cm^{-2}; $1.5 > E > 0.01$ GeV; $F_d = 22\%$. (d) Xe irradiation; $\phi t = 3.5 \times 10^{11}$ cm^{-2}; $3.0 > E > 0.15$ GeV; $F_d = 23\%$.

these two values have, on the contrary, been observed (present work compared to Ref. 9), when the fraction of disordered matter is higher than 50%, probably due to the magnetic phase transition occurring at room temperature. As a result, the values of F_d reported in Fig. 3(b) do not take into account the magnetization measurements and concern only the values deduced from the Mössbauer study.

V. DISCUSSION

A. Paramagnetic fraction

Assuming that the value of the paramagnetic fraction reflects a disorder induced only by atomic collisions, it appears that the number of displacements per atom is not able to put all the data on an unique curve (Fig. 3). This suggests that, for Kr and Xe irradiations, the electronic stopping power must be considered in the defect-creation mechanism.[12] However, for argon irradiation it should be noted, as shown by Chukalkin *et al.*[24–26] and Podsekin *et al.*,[27–29] that the same damage rate induced by neutron irradiation at 350 K is obtained for a number of displacement-per-atom of about 1–2 orders of magnitude higher, which, once again, suggests the strong influence of the electronic stopping power even for Ar ions, although the temperature effect has not been estimated.

The effect of the electronic stopping power is also corroborated by high-resolution electron microscopy (HREM) of samples irradiated by xenon ions in both $Y_3Fe_5O_{12}$ and $BaFe_{12}O_{19}$, which show the formation of continuous trails of damage.[12,14,30] These continuous trails of damage cannot be explained by elastic collisions since the mean free path between two collisions transferring at least 25 eV, is about 0.04 μm. Radii of 4.5 ± 1.0 and 4 ± 1 nm for $Y_3Fe_5O_{12}$ and $BaFe_{12}O_{19}$, respectively, have been measured on the HREM micrographies in good agreement with the values calculated from the disordered fraction following the relation (Ref. 8) $\pi R^2 \phi t = -\ln(1 - F_d)$. The track radii obtained from the averaged values of F_d have been plotted against $(dE/dx)^{1/3}$ in Fig. 7. The linear variation which can be observed for $Y_3Fe_5O_{12}$ irradiated by Xe and Kr ions is in good accord with the model proposed by Albrecht *et al.*[3] The extrapolation of the straight line to higher values of $(dE/dx)^{1/3}$ stands below the radii deduced from the experimental data of Hansen *et al.*[8] On the other hand, the extrapolation to lower values of $(dE/dx)^{1/3}$ suggests the existence of a threshold energy deposition of 17 MeV cm^2 mg^{-1} necessary to create latent tracks by electronic stopping power. Such a value is in good agreement with that deduced only from magnetization measurements[12] and could explain the low damage creation in $Y_3Fe_5O_{12}$ by Ar ions because the maximum electronic energy loss $(dE/dx)_e$ of Ar ions is 15.4 MeV cm^2 mg^{-1}. The enhancement of the disorder induced by Kr ions can thus be explained by electronic stopping.

In the case of $BaFe_{12}O_{19}$ only two points were deduced from the experimental data (Fig. 7). According to Al-

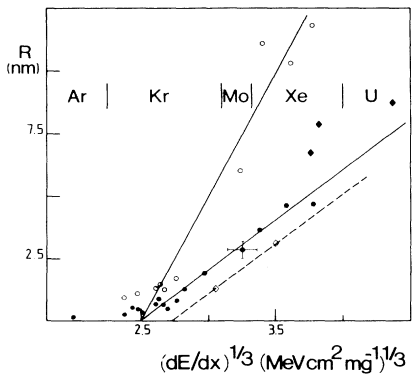

FIG. 7. Radii of latent tracks vs cubic root of the electronic stopping power. The point corresponding to a Mo irradiation has been added for comparison and will be published later.

brecht *et al.*, a line parallel to that of $Y_3Fe_5O_{12}$ has been drawn. Its extrapolation to low values of the electronic stopping power leads us to assume the existence of a threshold energy deposition of 25 MeV cm^2 mg^{-1}. Such a result would explain why, for $BaFe_{12}O_{19}$, no differences were observed between Ar and Kr irradiations when the energy loss was lower than 25 MeV cm^2 mg^{-1}, while a strong deviation [Fig. 3(b)] takes place when dE/dx is higher.

B. Orientation of the hyperfine magnetic field in $Y_3Fe_5O_{12}$

1. Argon Irradiations

As can be seen in Figs. 1(d) and 1(e), Ar irradiations tend to render the hyperfine magnetic field isotropic. The volume of the isotropic magnetic field region is 1 order of magnitude higher than that of the paramagnetic region. Assuming that the damaged regions are spheres, wherein the paramagnetic region is surrounded by a perturbed matrix with change of the magnetic field orientation, a ratio 2:1 has been found between the radius of both regions. It is well known from irradiation at low energy in $Y_3Fe_5O_{12}$ that the magnetic field direction tends to be parallel to the ion-induced stress.[31,32] In our case assuming that the irradiation creates defects with a low-density amorphous core surrounded by a high-density outer shell of interstitials, a spherical stress would take place around the defects, inducing an isotropic hyperfine magnetic field.

2. Xenon irradiations

In contrast to argon irradiations, Xe irradiations lead to an anisotropic distribution of the hyperfine field as pictured in Fig. 1(c). Then, the disordered region assumed to be a cylinder extending along the ion path, the presence of a transition region is reflected by the radius calculated from the orientation fraction and which appears to be twice that calculated from the paramagnetic fraction. According to the latent-track model of Hansen *et al.*,[8] the transition region could be a consequence of a linear stress parallel to the ion path induced by interstitial atoms expulsed from the central region of the latent tracks. A similar result has indeed been obtained by Hansen *et al.*[8] in thin $Y_3Fe_5O_{12}$ epitaxial layers irradiated by 0.38-GeV U ions with a very high electronic energy loss $(dE/dx)_e$, 73 MeV cm^2 mg^{-1}, whereas no change of orientation of the magnetic field has been observed with (0.2–0.8)-GeV Xe ions. An interpretation of these limited effects in the case of thin films could be found in the fact that the samples, and mainly the substrate, were not completely traversed, since the range, in the case of 0.38-GeV U ions, is limited to 30 μm.[8,33]

3. Krypton irradiations

As the range of the electronic stopping power of the Kr ions is intermediate between the two previous cases we shall now discuss it extensively. The results for the irradiation of a stack of disks by krypton ions of 3.5-GeV energy are shown in Fig. 2. For an electronic stopping power higher than 15 MeV cm^2 mg^{-1}, an anisotropic distribution of the hyperfine magnetic field is observed, as in xenon irradiation, together with the appearance of a paramagnetic fraction. As it has been realized for the paramagnetic fraction, the radius R_o of a cylinder containing the oriented part of the hyperfine magnetic field plus the paramagnetic fraction has been calculated and the values are reported for Kr and Xe ions versus the cubic root of the electronic stopping power. The straight line for the higher values of dE/dx (Fig. 7, curve 2), passing through these points allows to determine once more a threshold energy deposition for the efficiency of the electronic stopping power which is close to the value 17 MeV cm^2 mg^{-1} deduced from the paramagnetic fraction.

For the first sample of the preceding stacks of Kr irradiation, the mean electronic stopping-power value was 13.5 MeV cm^2 mg^{-1}. The experimental result is the same as in the case of Ar irradiation [Figs. 1(d) and 1(e)], i.e., a tendency to render isotropic the hyperfine magnetic field which is anisotropic in the nonirradiated single crystal. This result confirms the existence of a change in the electronic stopping-power damage: under the threshold value, the residual defects induce an isotropic distribution of the hyperfine magnetic field, whereas above that value an anisotropic distribution is observed.

This result seems to be in contradiction with the results of Albrecht *et al.*,[4] who show that there is no change in the defects above and under the threshold energy deposition for etching latent tracks. But, so far, we do not know the energy-deposition threshold for such etching latent tracks in $Y_3Fe_5O_{12}$.

C. Comparison with the available track models

1. Ion-explosion-spike model

The first model which has been proposed is based on Coulomb interactions between highly ionized atoms and hence called the ion-explosion-spike model.[34] In such a model it is assumed that there is a threshold ion-track sensitivity depending on the primary ionization rate. The volume of the extended-defect region is proportional to the electronic stopping power and inversely proportional to the product of the dielectric constant and Young modulus. According to Albrecht *et al.*,[3] the present results agree quite well since the radius of the cylinder of defects is proportional to the cubic root of dE/dx (Fig. 7) above the threshold. This is in agreement with previous work,[1–3,35,36] and with high-resolution-microscopy observations.[12,14,30]

2. Extended defects: K-shell ionization

The second model was based on the observation of the latent tracks by means of low-angle x-ray scattering.[37,1] The experimental results have been interpreted in terms of extended defects of diameter $\sim$3 nm separated by 20 nm, coupled with many much smaller and more numerous defects of a few atomic volumes in size. The induced damage[38] is initiated at separate points along the track by Auger decay of vacancies produced by the ion in the inner electronic shells of the atoms. The probability of finding extended defects measured by the paramagnetic fraction

or disordered fraction can be expressed versus the fluence ϕt as

$$F_d = 1 - \exp(-\sigma N_0 V \phi t) , \quad (1)$$

where σ is the cross section, N_0 the atomic density, and V the spherical volume of the extended defects contained in a sphere. Using a more recent formalism,[6,34,39] F_d can also be expressed as $F_d = 1 - \exp(-\lambda N_e)$, where $\lambda = V\phi t$ is the length and $N_e = \sigma N_0$ the number of extended defects. Using the binary-encounter approximation[39] in order to calculate the cross section σ_K for a K-shell ionization, previous results were explained using either (Refs. 1 and 40) a constant length λ or (Ref. 6) a length λ proportional to $(dE/dx)^{1/3}$ for the extended defect. In the present case, the values of $\lambda/2$ which characterize the radius of the extended defects induced by Kr irradiation (samples 9–12, Table I) have been reported in Table II. As can be seen, these values are neither constant nor proportional to $(dE/dx)^{1/3}$ (Ref. 6) and also too small compared to the experimental data (3 nm in Refs. 1 and 37). Moreover, using the largest values of the radius (Table II) the xenon data [Fig. 1(c)] cannot be reproduced. On the other hand, with $\lambda/2 = 0.5$ nm corresponding to sample 9 (Table II) irradiated by Kr ions, the value $F_d = 0.25$ is found for Ar irradiation using relation (1), in agreement with the experimental data [Fig. 1(b)]. However, it should be pointed out that such a result does not allow to explain the formation of Ar damage on the basis of the electronic stopping power since a scaling of these last two experimental data could be done using the elastic collision cross sections.

3. *Extended defects: Mean ionization of atomic shells*

The third model[5] is also based on the observation of extended defects, but supposing that one extended defect is the consequence of m_c successive ionizations. Therefore the probability of finding one extended defect along one track is expressed as

$$N_e\lambda = 1 - e^{-r\lambda}\left[\sum_{m=0}^{m_c-1}\frac{(r\lambda)^m}{m!}\right] ,$$

where N_e is the number per cm of extended defects of length λ, and r is the ionization cross section of a target atom with an energy[5] corresponding to the mean ionization potential.[41] It should be mentioned here that the second model corresponds to $m_c = 1$ and r to the K-shell ionization cross section. In this model, the disordered fraction F_d, which has been determined experimentally,

TABLE II. Radius of the extended defects determined using the second model (Ref. 37).

Sample	$\langle dE/dx \rangle$ (MeV cm^2 mg^{-1})	$\lambda/2$ (nm)	$(dE/dx)^{1/3}$
9	13.5	0.5	2.38
10	15.6	0.73	2.50
11	18.5	1	2.64
12	23.8	1.20	2.88

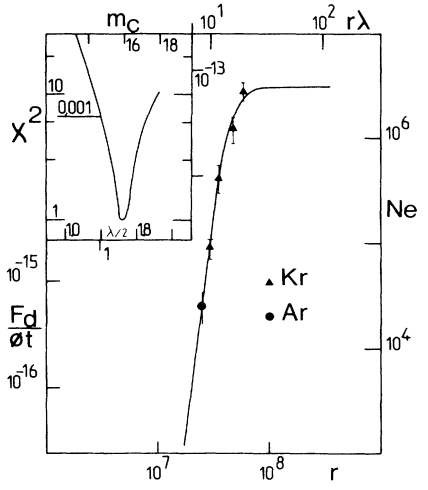

FIG. 8. F_d/t and N_e vs r or $r\lambda$ results of the krypton data fit. The inset corresponds to the χ^2 curve used to determine the best values of m_c and $\lambda/2$. $F_d/\phi t$ is the percentage of disordered fraction per ion, N_e is the number of events per cm, r is the number of ionization per cm, λ is in nm, and $r\lambda$ is without unity.

can be related to N_e by

$$F_d = 1 - \exp(-N_e V \phi t) ,$$

where V is the volume of a spherical defect of radius $\lambda/2$. Following the calculation described in Ref. 5, the parameters m and $\lambda/2$ have been adjusted in order to fit the experimental data using the χ^2 criterion. The results lead to the curve sketched in Fig. 8 and to the corresponding values of m_c and $\lambda/2$ equal to 16 ± 3 and 1.65 ± 0.30 nm, respectively, close to those obtained for Kr irradiation in mica.[5] With these values and errors, the probability that the difference between the experimental and calculated data exceeds 6, the value of the normalized χ^2, is 1%. Moreover, as can be seen in Fig. 8, the origin of the paramagnetic fraction observed in argon irradiation can be explained. On the contrary, this model is not able to describe the xenon data.

In Fig. 7, using the curve R-vs-$(dE/dx)^{1/3}$ data deduced from the paramagnetic fraction induced in $Y_3Fe_5O_{12}$, at $R = 1.65$ nm, equal to $\lambda/2$, the value of the electronic stopping power is 2.9 (MeV cm^2 mg^{-1})$^{1/3}$, i.e., 24.6 MeV cm^2 mg^{-1}. From this, a new definition of the threshold energy deposition for creation of latent tracks in a solid can then be considered. It takes into account the appearance of a continuous trail of damage instead of a mere extrapolation to a cylinder radius equal to zero. This new definition could be the one associated with the track-etching sensitivity. Thus this third model is able to explain defect creation by Ar and Kr irradiation, suggesting that they are a consequence of the electronic energy deposition.

VI. CONCLUSION

In addition to magnetization measurements, Mössbauer spectroscopy of $Y_3Fe_5O_{12}$ and $BaFe_{12}O_{19}$ oxides irradiated

with high-energy heavy ions throws light on the electronic stopping dependence of the induced damage. Thus the enhancement of the paramagnetic state created by Kr ions with respect to Ar ions can be explained on the basis of additional damage due to the energy deposited by electronic stopping. A track mechanism has been considered with the Xe ions to explain the damage rate since latent tracks have been observed by high-resolution electron microscopy in both $Y_3Fe_5O_{12}$ and $BaFe_{12}O_{19}$.

According to Albrecht,[3] a linear variation of the track radius deduced from the paramagnetic fraction, with the cubic root of the electronic energy loss, has been observed, which allows us to determine a threshold energy deposition for the creation of tracks: values of 17 and 25 MeV $cm^2\,mg^{-1}$ for $Y_3Fe_5O_{12}$ and $BaFe_{12}O_{19}$, respectively, show the influence of the nature of the chemical bond and structure on the damage rate by electronic energy loss.

Moreover, it has been shown that, whatever the defect mechanism may be, changes in the bulk orientation of the hyperfine magnetic field occur in $Y_3Fe_5O_{12}$. The distribution of the magnetic field is isotropic for Ar irradiations and anisotropic for Xe irradiations. For Kr irradiations the two types of distributions of the magnetic field have been observed, emphasizing the existence of a threshold energy deposition.

Finally, the explosion-spike model appears able to describe the damage induced above the threshold energy deposition when a continuous trail of damage is clearly established. If we consider the induced damage as being formed of isolated extended defects, the third model appears better than the second one to describe our experimental Kr- and Ar-irradiation data for an energy deposition around and smaller than 17 MeV $cm^{-2}\,mg^{-1}$. Moreover, it suggests that the damage induced by argon ions could also be a consequence of the electronic stopping power.

ACKNOWLEDGMENTS

This experiment was performed at National Laboratory Grand Accélérateur National d'Ions Lourds, Caen, France. We are grateful to Dr. E. Balanzat and J. C. Jousset (CIRIL, Caen, France) for stimulating discussion and to Dr. J. C. Greneche (Université du Maine, Le Mans, France) for enlightening criticisms on Mössbauer experimental results. Laboratoire de Cristallographie Physique et Chimie du Solide is unité associé No. 251. One of us (G.F.) was supported at CIRIL by a CEA/Department of Technology grant.

*Present address: Département Physique des Matériaux, Université C. Bernard Lyon I, bd. du 11 Novembre 1918, 69622 Villeurbanne, France.

[1]E. Dartyge, J. P. Duraud, Y. Langevin, and M. Maurette, Phys. Rev. B **38**, 5213 (1981).
[2]T. A. Tombrello, Nucl. Instrum. Methods B **2**, 555 (1984).
[3]D. Albrecht, P. Armbruster, R. Spohr, M. Roth, K. Schaupert, and H. Stuhrmann, Appl. Phys. A **37**, 37 (1985).
[4]D. Albrecht, E. Balanzat, and K. Schaupert, Nucl. Tracks Radiat. Meas. **11**, 93 (1986).
[5]E. Dartyge and P. Sigmund, Phys. Rev. B **32**, 5249 (1985).
[6]T. A. Tombrello, Nucl. Instrum. Methods B **1**, 23 (1984).
[7]P. Hansen and H. Heitmann, Phys. Rev. Lett. **43**, 1444 (1979).
[8]P. Hansen, H. Heitmann, and P. M. Smit, Phys. Rev. B **26**, 3539 (1982).
[9]D. Groult, M. Hervieu, N. Nguyen, B. Raveau, G. Fuchs, and E. Balanzat, Radiat. Eff. **90**, 19 (1982).
[10]G. Fuchs, F. Studer, E. Balanzat, D. Groult, J. C. Jousset, and B. Raveau, Nucl. Instrum. Methods B **12**, 471 (1985).
[11]G. Fuchs, thèse troiseme cycle, Université de Caen, 1985, Commissariat á l'Energie Atomique Report No. R5343, 1986 (unpublished).
[12]G. Fuchs, F. Studer, E. Balanzat, D. Groult, M. Toulemonde, and J. C. Jousset, Europhys. Lett. **3**, 321 (1987).
[13]F. Studer, D. Groult, N. Nguyen, and M. Toulemonde, Nucl. Instrum. Methods B **19/20**, 856 (1987).
[14]G. Fuchs, D. Groult, M. Hervieu, N. Nguyen, F. Studer, M. Toulemonde, and B. Raveau, in Proceedings of the Third European Conference on Solid State Chemistry Regensburg, 1986 (unpublished).
[15]J. Dural and J. M. Ramillon (private communication).
[16]A. Dael, X. Dugay, M. Duval, C. Eveillard, J. Lebourdie, A. Lemarie, J. P. Libin, and M. Ohayon, GANIL Internal Report No. 84N/019/MAG/04, 1984 (unpublished).
[17]M. Toulemonde and A. Dunlop, note technique, CIRIL Report No. 85/227, 1985 (unpublished).
[18]H. Winkler, R. Eisberg, E. Alp, R. Rüffer, E. Gerdau, S. Lauer, A. X. Trautwein, M. Grodzicki, and A. Vera, Z. Phys. B **49**, 331 (1983).
[19]J. G. Rensen and J. S. Wieringen, Solid State Commun. 1139 (1969).
[20]E. Kreber and U. Gonser, Appl. Phys. **10**, 175 (1976).
[21]F. Studer, N. Nguyen, G. Fuchs, and M. Toulemonde, Hyperfine Interact. **29**, 1287 (1986).
[22]M. Toulemonde, D. Groult, N. Nguyen, and F. Studer, in *European Materials Research Society Conference, Strasbourg, 1986,* edited by R. Krishnan (Les Editions de Physique, Paris, 1986), p. 121.
[23]N. J. Norgett, M. T. Robinson, and I. M. Torrens, Nucl. Eng. Des. **33**, 50 (1975).
[24]Yu.G. Chukalkin, B. N. Goshchitskii, S. K. Sidorov, V. V. Petrov, V. D. Parlhomenko, and V. G. Vologin, Phys. Status Solidi A **28**, 345 (1975).
[25]Yu.G. Chukalkin, V. V. Petrov, and B. N. Goshchitskii, Phys. Status Solid A **67**, 421 (1981).
[26]Yu.G. Chukalkin, V. R. Shtirts, and B. N. Goshchitskii, Phys. Status Solidi A **79**, 361 (1983).
[27]A. K. Podsekin and V. A. Sarin, Z. Tekh. Fiz. **51**, 981 (1981) [Sov. Phys.—Tech. Phys. **26**, 586 (1981)].
[28]A. K. Podsekin and V. N. Zaitsev, Fiz. Tverd. Tela. (Leningrad) **24**, 607 (1982) [Sov. Phys.—Solid State **24**, 342 (1982)].
[29]A. K. Podsekin, V. N. Zaitsev, and I. I. Kuz'min, Zh. Tekh. Fiz. **52**, 87 (1982) [Sov. Phys.—Tech. Phys. **27**, 54 (1982)].
[30]M. Toulemonde and F. Studer (private communication).
[31]P. Gerard, Thin Solid Films **114**, 3 (1984).
[32]G. Marest, A. Perez, J. L. Ponthenier, P. Gerard, and J. M. Roberston, J. Appl. Phys. **55**, 2560 (1984).

[33]B. Strocka, G. Bartels, and R. Spohr, Appl. Phys. **21**, 141 (1980).
[34]R. L. Fleischer, P. B. Price, and R. M. Walker, *Nuclear Tracks in Solids* (University of California Press, Berkeley, 1975).
[35]T. A. Tombrello, C. R. Wie, N. Itoh, and T. Nakayama, Phys. Lett. **100A**, 42 (1984).
[36]Y. Qiu, J. E. Griffith, J. M. Meng, and T. A. Tombrello, Radiat. Eff. **70**, 231 (1983).
[37]M. Lambert, A. M. Levelut, M. Maurette, and H. Heckman, Radiat. Eff. **3**, 155 (1970).
[38]M. Maurette, Radiat. Eff. **3**, 149 (1970).
[39]J. D. Garcia, R. J. Fortner, and T. M. Kavanagh, Rev. Mod. Phys. **45**, 111 (1973).
[40]J. P. Duraud, Ph.D. thesis, Université de Paris–Sud, 1978, No. 2086 (unpublished).
[41]U. Fano, Annu. Rev. Nucl. Sci. **13**, 1 (1963).